On Shape Optimization with Parabolic State Equation

Helmut Harbrecht, Johannes Tausch

Institute of Mathematics
University of Basel
Rheinsprung 21
CH - 4051 Basel
Switzerland

Preprint No. 2013-23
September, 2013

www.math.unibas.ch

On shape optimization with parabolic state equation

Helmut Harbrecht and Johannes Tausch

Abstract The present paper intends to summarize the main results of [17, 18] on the numerical solution of shape optimization problems for the heat equation. This is carried out by means of a specific problem, namely the reconstruction of a heat source which is located inside the computational domain under consideration from measurements of the heat flux through the boundary. We arrive at a shape optimization problem by tracking the mismatch of the heat flux at the boundary. For this shape functional, the Hadamard representation of the shape gradient is derived by use of the adjoint method. The state and its adjoint equation are expressed as parabolic boundary integral equations and solved using a Nyström discretization and a space-time fast multipole method for the rapid evaluation of thermal potentials. To demonstrate the similarities to shape optimization problems for elliptic state equations, we consider also the related stationary shape optimization problem which involves the Poisson equation. Numerical results are given to illustrate the theoretical findings.

1 Introduction

Shape optimization is a well established mathematical and computational tool in case of an elliptic state equation, see e.g., [2, 13, 14, 19, 25, 26, 28, 29, 32, 33] and the references therein. In contrast, the literature on shape optimization is rather limited for a parabolic state equation. Theoretical results for the latter case can be found, for instance, in [4, 20, 21, 31] and the references therein. However, the development of efficient numerical methods for shape optimization problems with a parabolic

Helmut Harbrecht
Mathematisches Institut, Universität Basel, Rheinsprung 21, 4051 Basel, Schweiz
e-mail: helmut.harbrecht@unibas.ch

Johannes Tausch
Department of Mathematics, Southern Methodist University, Dallas, Texas, USA
e-mail: tausch@smu.edu

state equation is still in its beginning stages, especially for three-dimensional geometries.

With the goal to develop such efficient methods, we considered in [17, 18] shape identification problems for the heat equation. Specifically, besides the computation of the Hadamard representation of the shape gradients, we applied boundary integral equations to provide that data from the state and its adjoint which enter the shape functional and shape gradient. These boundary integral equations have been solved by multipole-based space-time boundary element methods which cluster sources in space and time have become available recently [34, 35]. That way, we were able to reconstruct unknown shapes in three dimensions on a laptop in less than half an hour computation time even though up to 1200 design parameters and about 120 000 boundary elements have been used for the discretization of the shape optimization problem.

If one takes a closer look at [17, 18], it turns out that for a parabolic state equation both, the shape calculus and the formulation by boundary integral equations, are in principle rather similar to the case of an elliptic state equation. Besides being numerically more challenging, the main difference is that in the parabolic case singularities appear since the initial data do not generally fit the given boundary data, especially in the adjoint state equation. The similarities stem from the fact that the sought shape has not been allowed to change in time. Future research should thus go into the direction of shape optimization problems where the shape varies in time.

The present paper intends to summarize the main results of [17, 18] by focusing on a specific shape reconstruction problem with parabolic state equation. The goal is to reconstruct the shape of a heat source inside a given domain from the knowledge of the temperature and the heat flux at the boundary of the domain. We provide the ingredients (shape gradient, discretization of the shape, discretization of the state equation and its adjoint) for an efficient shape reconstruction algorithm and compare them with the ingredients for the related stationary problem which is obtained by letting time tend to infinity.

The paper is organized as follows. In Section 2, the problems under consideration are formulated. The Hadamard representation of the shape gradients is derived in Section 3. The following section describes the discretization of the shape. The computation of the state and the adjoint state by boundary integral equations is proposed in Section 5. Finally, in Section 6, we compare the reconstruction of shapes in case of the elliptic state equation with the reconstruction of shapes in case of the parabolic state equation.

2 Problem formulation

The shape identification problem under consideration is as follows. Let D be a domain contained in a domain $\Omega \subset \mathbb{R}^3$ and consider the initial boundary value problem

$$\partial_t u - \Delta u = \chi_D \quad \text{in } \Omega \times (0,T) \tag{1}$$

with boundary condition

$$u = 0 \quad \text{on } \Sigma \times (0,T) \tag{2}$$

and initial condition

$$u = 0 \quad \text{on } \Omega \times \{0\}. \tag{3}$$

Here, $\Sigma = \partial\Omega$ denotes the boundary of the domain Ω, whereas we will denote the boundary of D by $\Gamma := \partial D$, see also Figure 1. Throughout the paper, we assume that the boundaries Σ and Γ are respectively Lipschitz-continuous and C^2-smooth.

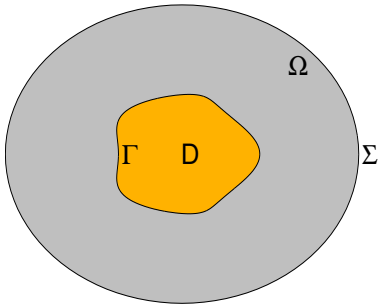

Fig. 1 The domain Ω with boundary Σ and the source D with boundary Γ.

The goal is to reconstruct the discontinuous source D from measurements of the Neumann data $\partial u/\partial \mathbf{n}$ at the boundary Σ. More precisely, we will minimize the least square functional

$$J(D) = \frac{1}{2}\int_0^T \int_\Sigma \left(\frac{\partial u}{\partial \mathbf{n}} - h\right)^2 \mathrm{d}\sigma\,\mathrm{d}t \to \inf. \tag{4}$$

This problem has firstly been considered by Hettlich and Rundell in [23] and is known to be severely ill-posed. Since we track the Neumann data over the whole boundary Σ, uniqueness of the solution D immediately follows from [24], where the steady state case has been considered, governed by the equation (5) below. Nevertheless, uniqueness can be proven under much milder assumptions, see [23] and the references therein.

For comparison reasons, we shall also consider the steady state case which is obtained for $T \to \infty$. Then, the state equation (1) simplifies to the Poisson equation

$$-\Delta u = \chi_D \quad \text{in } \Omega, \tag{5}$$

while the initial condition (3) disappears and the boundary condition (6) becomes

$$u = 0 \quad \text{on } \Sigma. \tag{6}$$

The analogue of the shape functional (4) reads now as

$$J(D) = \frac{1}{2}\int_\Sigma \left(\frac{\partial u}{\partial \mathbf{n}} - h\right)^2 \mathrm{d}\sigma \to \inf. \tag{7}$$

To the best of our knowledge, this problem has not been considered before in the literature.

We will demonstrate the similarities between the shape calculus of the transient and the steady state case, using the shape identification problems (4) and (7). Both cost functionals (4) and (7) can be minimized by means of gradient based iterative methods. To this end, we need to compute the Hadamard representations of the shape gradients. They are obtained by applying the so-called adjoint method. The shape gradients are scalar distributions on the free boundary Γ, involving in general only information of the state and the associated adjoint state.

3 Computing the shape gradients

Shape calculus has to be used to derive the shape gradients of the shape optimization problems under considerations. For a general overview on shape calculus, mainly based on the perturbation of identity (Murat and Simon) or the speed method (Sokolowski and Zolesio), we refer the reader for example to [2, 27, 28, 30, 32] and the references therein.

The shape gradient of the cost functional (4) with parabolic state equation (1)–(3) is given in the following theorem which has been proven in [17]. Nevertheless, we present its proof here for the sake of completeness. In particular, a comparison with the proof of Theorem 2 reveals clearly the similarities to the derivation of the shape gradient of the associated cost functional (7) with elliptic state equation (5) and (6).

Theorem 1. *For an arbitrary boundary perturbation field $\mathbf{V} \in C^2(\Gamma)$, the shape gradient to the cost functional* (4) *with parabolic state equation* (1)–(3) *reads as*

$$\delta J(D)[\mathbf{V}] = -\int_0^T \int_\Gamma \langle \mathbf{V}, \mathbf{n}\rangle p \,\mathrm{d}\sigma \,\mathrm{d}t, \tag{8}$$

where p denotes the adjoint state which satisfies the adjoint state equation

$$\begin{aligned} -\partial_t p - \Delta p &= 0 && \text{in } \Omega\times(0,T),\\ p &= \frac{\partial u}{\partial \mathbf{n}} - h && \text{on } \Sigma\times(0,T),\\ p &= 0 && \text{on } \Omega\times\{T\}. \end{aligned} \tag{9}$$

Proof. Given an arbitrary boundary perturbation field $\mathbf{V} \in C^2(\Gamma)$, the directional derivative of the cost functional (4) is

$$\delta J(D)[\mathbf{V}] = \int_0^T \int_\Sigma \left(\frac{\partial u}{\partial \mathbf{n}} - h\right) \frac{\partial \delta u}{\partial \mathbf{n}} \,\mathrm{d}\sigma \,\mathrm{d}t$$

with $\delta u = \delta u[\mathbf{V}]$ denoting the local shape derivative. According to [23], it satisfies the following coupled initial boundary value problem

$$\begin{aligned}
\partial_t \delta u_e - \Delta \delta u_e &= 0 && \text{in } (\Omega \setminus \overline{D}) \times (0,T),\\
\partial_t \delta u_i - \Delta \delta u_i &= 0 && \text{in } D \times (0,T),\\
\delta u_e &= 0 && \text{on } \Sigma \times (0,T),\\
\delta u_e = \delta u_i,\ \frac{\partial \delta u_e}{\partial \mathbf{n}} &= \frac{\partial \delta u_i}{\partial \mathbf{n}} + \langle \mathbf{V}, \mathbf{n} \rangle && \text{on } \Gamma \times (0,T),\\
\delta u_e &= 0 && \text{on } (\Omega \setminus \overline{D}) \times \{0\},\\
\delta u_i &= 0 && \text{on } D \times \{0\}.
\end{aligned} \tag{10}$$

Observing (9) and (10), integration by parts leads to

$$\begin{aligned}
0 &= \int_0^T \int_{\Omega \setminus \overline{D}} (\partial_t \delta u_e - \Delta \delta u_e) p + (\partial_t p + \Delta p) \delta u_e \, \mathrm{d}\mathbf{x} \, \mathrm{d}t \\
&= \int_{\Omega \setminus \overline{D}} \int_0^T \{ \partial_t \delta u_e p + \delta u_e \partial_t p \} \, \mathrm{d}t \, \mathrm{d}\mathbf{x} - \int_0^T \int_{\Omega \setminus \overline{D}} \{ \Delta \delta u_e p - \delta u_e \Delta p \} \, \mathrm{d}\mathbf{x} \, \mathrm{d}t \\
&= \int_{\Omega \setminus \overline{D}} \Big\{ \underbrace{\delta u_e(\cdot,T) p(\cdot,T) - \delta u_e(\cdot,0) p(\cdot,0)}_{=0} \Big\} \, \mathrm{d}\mathbf{x} \\
&\qquad + \int_0^T \int_{\Sigma \cup \Gamma} \left\{ \delta u_e \frac{\partial p}{\partial \mathbf{n}} - \frac{\partial \delta u_e}{\partial \mathbf{n}} p \right\} \mathrm{d}\sigma \, \mathrm{d}t.
\end{aligned}$$

In view of $\delta u_e = 0$ on $\Sigma \times (0,T)$, this implies

$$\delta J(D)[\mathbf{V}] = \int_0^T \int_\Sigma \frac{\partial \delta u_e}{\partial \mathbf{n}} p \, \mathrm{d}\sigma \, \mathrm{d}t = \int_0^T \int_\Gamma \left\{ \frac{\partial \delta u_e}{\partial \mathbf{n}} p - \delta u_e \frac{\partial p}{\partial \mathbf{n}} \right\} \mathrm{d}\sigma \, \mathrm{d}t. \tag{11}$$

In complete analogy to above, we find again by integration by parts

$$\begin{aligned}
0 &= \int_0^T \int_D (\partial_t \delta u_i - \Delta \delta u_i) p + (\partial_t p + \Delta p) \delta u_i \, \mathrm{d}\mathbf{x} \, \mathrm{d}t \\
&= \int_0^T \int_\Gamma \left\{ \delta u_i \frac{\partial p}{\partial \mathbf{n}} - \frac{\partial \delta u_i}{\partial \mathbf{n}} p \right\} \mathrm{d}\sigma \, \mathrm{d}t.
\end{aligned}$$

Due to the jump condition of δu at Γ, we thus conclude

$$0 = \int_0^T \int_\Gamma \left\{ \delta u_e \frac{\partial p}{\partial \mathbf{n}} + \left(\langle \mathbf{V}, \mathbf{n} \rangle - \frac{\partial \delta u_e}{\partial \mathbf{n}} \right) p \right\} \mathrm{d}\sigma \, \mathrm{d}t,$$

cf. (10). Inserting this equation into (11) yields finally (8). □

In case of the shape optimization problem (7) with elliptic state equation (5) and (6), we obtain the following shape gradient. Here, the underlying operator of the elliptic state equation is self adjoint, and, thus, the adjoint state equation involves the same operator as the primal state equation.

Theorem 2. *For an arbitrary boundary perturbation field* $\mathbf{V} \in C^2(\Gamma)$*, the shape gradient to the cost functional* (7) *with elliptic state equation* (5) *and* (6) *reads as*

$$\delta J(D)[\mathbf{V}] = -\int_\Gamma \langle \mathbf{V}, \mathbf{n} \rangle p \, \mathrm{d}\sigma, \tag{12}$$

where p denotes the adjoint state which satisfies the adjoint state equation

$$\begin{aligned} \Delta p &= 0 && \text{in } \Omega, \\ p &= \frac{\partial u}{\partial \mathbf{n}} - h && \text{on } \Sigma. \end{aligned} \tag{13}$$

Proof. The proof uses the same arguments as the proof of Theorem 1. For an arbitrary boundary perturbation field $\mathbf{V} \in C^2(\Gamma)$, we find the directional derivative

$$\delta J(D)[\mathbf{V}] = \int_\Sigma \left(\frac{\partial u}{\partial \mathbf{n}} - h \right) \frac{\partial \delta u}{\partial \mathbf{n}} \, \mathrm{d}\sigma$$

with $\delta u = \delta u[\mathbf{V}]$ satisfying the coupled boundary value problem (cf. [22])

$$\begin{aligned} \Delta \delta u_e &= 0 && \text{in } \Omega \setminus \overline{D}, \\ \Delta \delta u_i &= 0 && \text{in } D, \\ \delta u_e &= 0 && \text{on } \Sigma, \\ \delta u_e = \delta u_i, \ \frac{\partial \delta u_e}{\partial \mathbf{n}} &= \frac{\partial \delta u_i}{\partial \mathbf{n}} + \langle \mathbf{V}, \mathbf{n} \rangle && \text{on } \Gamma. \end{aligned} \tag{14}$$

Integration by parts gives in view of (13) and (14)

$$0 = \int_{\Omega \setminus \overline{D}} \Delta p \delta u_e - \Delta \delta u_e p \, \mathrm{d}\mathbf{x} = \int_{\Sigma \cup \Gamma} \left\{ \delta u_e \frac{\partial p}{\partial \mathbf{n}} - \frac{\partial \delta u_e}{\partial \mathbf{n}} p \right\} \mathrm{d}\sigma$$

and, since $\delta u_e = 0$ on Σ, thus

$$\delta J(D)[\mathbf{V}] = \int_\Sigma \frac{\partial \delta u_e}{\partial \mathbf{n}} p \, \mathrm{d}\sigma = \int_\Gamma \left\{ \frac{\partial \delta u_e}{\partial \mathbf{n}} p - \delta u_e \frac{\partial p}{\partial \mathbf{n}} \right\} \mathrm{d}\sigma. \tag{15}$$

Using next integration by parts on the domain D, we likewise conclude

$$0 = \int_D \Delta p \delta u_i - \Delta \delta u_i p \, \mathrm{d}\mathbf{x} = \int_\Gamma \left\{ \delta u_i \frac{\partial p}{\partial \mathbf{n}} - \frac{\partial \delta u_i}{\partial \mathbf{n}} p \right\} \mathrm{d}\sigma.$$

The jump condition of δu at Γ (cf. (14)) implies

$$0 = \int_\Gamma \left\{ \delta u_e \frac{\partial p}{\partial \mathbf{n}} + \left(\langle \mathbf{V}, \mathbf{n} \rangle - \frac{\partial \delta u_e}{\partial \mathbf{n}} \right) p \right\} \mathrm{d}\sigma,$$

which, together with (15), shows finally (12). □

With the help of the Hadamard representations (8) and (12) of the shape gradients, we are able to develop efficient gradient based algorithms for the minimization of the cost functionals (4) and (7), respectively.

4 Discretization of the free boundary

In order to solve the shape optimization problems under consideration we seek a stationary point $D^\star$, being C^2-smooth, which satisfies

$$\delta J(D^\star)[\mathbf{V}] = 0 \text{ for all } \mathbf{V} \in C^2(\Gamma). \tag{16}$$

This is called the necessary optimality condition of the shape optimization problem $J(D^\star) \to \inf$. For related sufficient optimality conditions, we refer the reader to [9, 13] and the references therein. Nevertheless, we emphasize that, in the current context of severely ill-posed problems, sufficient optimality conditions cannot hold since the adjoint state vanishes in the optimal domain $D^\star$.

4.1 Nonlinear Ritz-Galerkin approximation for the shape

From now on we restrict ourselves to the practically most important case of $n = 3$ and consider the minimization of the cost functional over heat sources that are topologically equivalent to the unit sphere $\mathbb{S}^2$. Then, we can represent the heat source $D \subset \mathbb{R}^3$ by a parameterization

$$\gamma = (\gamma_1, \gamma_2, \gamma_3) : \mathbb{S}^2 \to \Gamma, \tag{17}$$

which is one-to-one, preserves orientation, and the Jacobian matrix $\gamma'(\widehat{\mathbf{x}})$ is invertible for all $\widehat{\mathbf{x}} \in \widehat{\Gamma}$. By restricting the parameterization to a finite dimensional ansatz space V_N, we arrive at the nonlinear Ritz-Galerkin scheme for (16):

$$\text{Seek } \gamma_N^\star \in V_N \text{ such that } \delta J(\gamma_N^\star)[\mathbf{V}_N] = 0 \text{ for all } \mathbf{V}_N \in V_N. \tag{18}$$

For the numerical solution of the nonlinear variational problem (18), we apply the quasi-Newton method, updated by the inverse BFGS-rule without damping. A second order approximation is used for performing the line search update if the descent does not satisfy the Armijo rule. Since we use a gradient based iterative method, regularization is not necessary provided that we stop the iteration early enough. For all the details and a survey on available optimization algorithms, we refer to [3, 10, 11, 12] and the references therein.

Following [17, 18], we can distinguish two types of parameterizations. The first type is of the form

$$\gamma(\widehat{\mathbf{x}}) = r(\widehat{\mathbf{x}}) \cdot \widehat{\mathbf{x}}, \quad r \in C^2(\mathbb{S}^2) \tag{19}$$

and is able to represent any given star-shaped source with center in $\mathbf{0}$. The discretization of Γ is based on the ansatz

$$r_N(\widehat{\mathbf{x}}) = \sum_{n=0}^{N} \sum_{m=-n}^{n} a_n^m Y_n^m(\widehat{\mathbf{x}}), \quad \widehat{\mathbf{x}} \in \mathbb{S}^2,$$

where $a_n^m \in \mathbb{R}$ are the design parameters and $Y_n^m \in C^\infty(\mathbb{S}^2)$ denote the spherical harmonic functions of degree n and order m. This leads to the finite dimensional parameterization

$$\gamma_N(\widehat{\mathbf{x}}) = r_N(\widehat{\mathbf{x}}) \cdot \widehat{\mathbf{x}}, \quad \widehat{\mathbf{x}} \in \mathbb{S}^2. \tag{20}$$

The advantage of this approach is that the identification of the function r_N, given by the design parameters, and the heat source is one-to-one. In particular, the distance between two domains can be simply measured via the ℓ^2-norm of the difference of the associated design parameters. This approach is used in our numerical example.

The second type, also referred to as flexible shape representation, allows a more general boundary representation than the somehow restrictive approach (19). Namely, we choose

$$\gamma_N(\widehat{\mathbf{x}}) = \sum_{n=0}^{N} \sum_{m=-n}^{n} \mathbf{a}_n^m Y_n^m(\widehat{\mathbf{x}}), \quad \widehat{\mathbf{x}} \in \mathbb{S}^2, \tag{21}$$

where $\mathbf{a}_i \in \mathbb{R}^3$ are *vector valued* design parameters. The ansatz (21) does not impose any restriction to the topology of the domain except for its genus. However, we lose the one-to-one correspondence between the shape of the heat source and the design parameters. Thus, a regularization of the shape function (see e.g. [13, 16, 17]) or a suitable remeshing algorithm (see e.g. [18]) needs to be applied.

4.2 Surface mesh generation

We shall assume that the boundary manifold $\Gamma \subset \mathbb{R}^3$ is given as a parametric surface consisting of smooth patches. More precisely, let $\square := [0,1]^2$ denote the unit square. The manifold Γ is partitioned into a finite number of *patches*

$$\Gamma = \bigcup_{i=1}^{M} \Gamma_i, \qquad \Gamma_i = \kappa_i(\square), \qquad i = 1,2,\ldots,M, \tag{22}$$

where each $\kappa_i : \square \to \Gamma_i$ defines a diffeomorphism of $\square$ onto Γ_i. The intersection $\Gamma_i \cap \Gamma_{i'}$, $i \neq i'$, of two patches Γ_i and $\Gamma_{i'}$ is assumed to be either $\emptyset$, or a common edge, or a common vertex. A mesh of the boundary Γ is then obtained by mapping a mesh of $\square$ to Γ via a parametrization.

The construction of the parametric representation of the moving boundary Γ should be presented in more detail. The surface of the cube $[-0.5,0.5]^3$ consists of

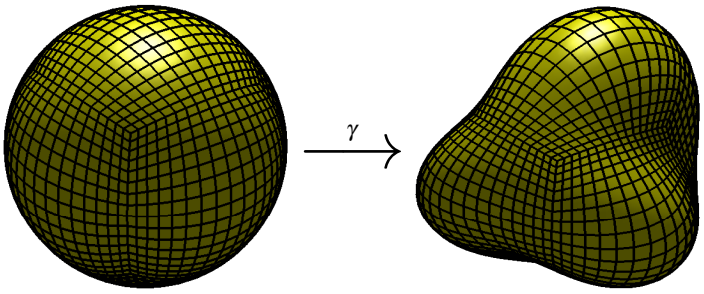

Fig. 2 Parametric representation of Γ with triangular mesh on level 4.

six patches. Each point $\mathbf{x} \in \partial([-0.5,0.5]^3)$ can be lifted onto the boundary Γ via the operation

$$\mathbf{y}(\mathbf{x}) = \gamma\left(\frac{\mathbf{x}}{\|\mathbf{x}\|}\right) \in \Gamma. \tag{23}$$

In this manner, the boundary Γ is subdivided into $M = 6$ patches. The parametric representations $\kappa_i : \square \to \Gamma_i$ can be derived easily from (23). Finally, we construct a mesh of Γ, required for the boundary element method, by mapping a triangular or quadrangular mesh of the unit cube via the sphere to Γ. We refer to Figure 2 for an illustration of the proposed parametric representation and mesh generation.

We shall finally specify how to distinguish between "nice" and "bad" parametrizations. A "nice" parametrization maps orthonormal tangents of the unit cube onto orthogonal tangents of length $\approx |\Gamma|/6$ with respect to the boundary Γ. This means that the first fundamental tensor of differential geometry, given by

$$\mathbf{S}_i(\mathbf{s}) = \left[\langle \kappa_{i,j}(\mathbf{s}), \kappa_{i,k}(\mathbf{s})\rangle\right]_{j,k=1,2}, \quad \mathbf{s} = [s_1, s_2]^T \in \square,$$

satisfies $\mathbf{S}_i \approx |\Gamma|/6 \cdot \mathbf{I}$. Hence, one can employ the shape functional

$$M(\gamma) = \sum_{i=1}^{6} \int_{\square} \left\| \begin{bmatrix} \langle \kappa_{i,1}(\mathbf{s}), \kappa_{i,1}(\mathbf{s})\rangle - \frac{|\Gamma|}{6} & \langle \kappa_{i,1}(\mathbf{s}), \kappa_{i,2}(\mathbf{s})\rangle \\ \langle \kappa_{i,2}(\mathbf{s}), \kappa_{i,1}(\mathbf{s})\rangle & \langle \kappa_{i,2}(\mathbf{s}), \kappa_{i,2}(\mathbf{s})\rangle - \frac{|\Gamma|}{6} \end{bmatrix} \right\|_F^2 \mathrm{d}\mathbf{s}$$

for regularizing the shape functional or as the base of a remeshing procedure.

5 Numerical method to compute the state and its adjoint

We shall discuss the numerical solution of the state equations and their adjoints by boundary element methods. With this technique only the boundaries of Ω an D need to be discretized, which avoids the complicated triangulation of the domain Ω with the varying source D. In particular, in case of the parabolic state equation, we

immediately arrive at a space-time formulation. This is very advantageous since the solution's complete temporal history which enters the adjoint state, being reverse in time, is available.

5.1 Solving the heat equation

The thermal layer operators are given by

$$\begin{aligned}
(\mathscr{V}g)(\mathbf{x},t) &= \int_0^t \int_\Sigma G(\|\mathbf{x}-\mathbf{y}\|,t-\tau)g(\mathbf{y},\tau)\,\mathrm{d}\sigma_\mathbf{y}\,\mathrm{d}\tau,\\
(\mathscr{K}g)(\mathbf{x},t) &= \int_0^t \int_\Sigma \frac{\partial G}{\partial \mathbf{n}_\mathbf{y}}(\|\mathbf{x}-\mathbf{y}\|,t-\tau)g(\mathbf{y},\tau)\,\mathrm{d}\sigma_\mathbf{y}\,\mathrm{d}\tau,\\
(\mathscr{K}^\star g)(\mathbf{x},t) &= \int_0^t \int_\Sigma \frac{\partial G}{\partial \mathbf{n}_\mathbf{x}}(\|\mathbf{x}-\mathbf{y}\|,t-\tau)g(\mathbf{y},\tau)\,\mathrm{d}\sigma_\mathbf{y}\,\mathrm{d}\tau,\\
(\mathscr{W}g)(\mathbf{x},t) &= -\frac{\partial}{\partial \mathbf{n}_\mathbf{x}} \int_0^t \int_\Sigma \frac{\partial G}{\partial \mathbf{n}_\mathbf{y}}(\|\mathbf{x}-\mathbf{y}\|,t-\tau)g(\mathbf{y},\tau)\,\mathrm{d}\sigma_\mathbf{y}\,\mathrm{d}\tau,
\end{aligned} \tag{24}$$

where $(\mathbf{x},t) \in \Sigma \times [0,T]$ and $G(\cdot,\cdot)$ is the heat kernel, given by

$$G(r,t) = \frac{1}{(4\pi t)^{3/2}} \exp\left(-\frac{r^2}{4t}\right).$$

With these boundary integral operators at hand, Green's representation formulae for the interior heat equation with homogeneous initial conditions can be written as

$$\left(\frac{1}{2}+\mathscr{K}\right)u - \mathscr{V}\frac{\partial u}{\partial \mathbf{n}} = \mathscr{N} \quad \text{and} \quad \left(\frac{1}{2}+\mathscr{K}^\star\right)\frac{\partial u}{\partial \mathbf{n}} + \mathscr{W}u = -\frac{\partial \mathscr{N}}{\partial \mathbf{n}}, \tag{25}$$

where $\mathscr{N}$ denotes the thermal Newton potential of the inhomogeneity. It is nonzero and, in accordance with [17], given by

$$\mathscr{N}(\mathbf{x},t) := \int_0^t \int_D G(\|\mathbf{x}-\mathbf{y}\|,t-\tau)\,\mathrm{d}\mathbf{y}\,\mathrm{d}\tau = \int_\Gamma \frac{\partial H}{\partial \mathbf{n}_\mathbf{y}}(\|\mathbf{x}-\mathbf{y}\|,t)\,\mathrm{d}\sigma_\mathbf{y},$$

where the kernel $H(\cdot,\cdot)$ is defined as

$$H(r,t) = \frac{2\sqrt{t}}{(4\pi)^{3/2}}\left[\sqrt{\pi}\,\mathrm{erfc}\left(\frac{r}{2\sqrt{t}}\right)\left(\frac{r}{2\sqrt{t}}+\frac{\sqrt{t}}{r}\right)+\exp\left(-\frac{r^2}{4t}\right)\right]. \tag{26}$$

Since the temperature satisfies $u=0$ at Σ, the unknown heat flux $\partial u/\partial \mathbf{n}$ at Σ can be derived from the boundary integral equations (25). Thus

$$-\mathscr{V}\frac{\partial u}{\partial \mathbf{n}} = \mathscr{N} \quad \text{and} \quad \left(\frac{1}{2}+\mathscr{K}^\star\right)\frac{\partial u}{\partial \mathbf{n}} = -\frac{\partial \mathscr{N}}{\partial \mathbf{n}}. \tag{27}$$

We will employ the second boundary integral equation for our shape reconstruction scheme. Nevertheless, the first boundary integral equation will be used to compute synthetic data in order to avoid an inverse crime.

For the computation of the solution of the state adjoint equation, we first perform the change of variables $t \mapsto T - t$ to obtain it in a more familiar form:

$$\begin{aligned} \partial_t \widetilde{p} - \Delta \widetilde{p} &= 0 \qquad \text{in } \Omega \times (0,T), \\ \widetilde{p} &= f \qquad \text{on } \Sigma \times (0,T), \\ \widetilde{p} &= 0 \qquad \text{on } \Omega \times \{0\}. \end{aligned} \tag{28}$$

Here, $\widetilde{p}(\mathbf{x},t) = p(\mathbf{x},T-t)$ and

$$f(\mathbf{x},t) = \frac{\partial u}{\partial \mathbf{n}}(\mathbf{x},T-t) - h(\mathbf{x},T-t).$$

It is convenient to use the indirect method where the solution is written as a double layer potential

$$\widetilde{p}(\mathbf{x},t) = \int_0^t \int_\Sigma \frac{\partial G}{\partial \mathbf{n}_\mathbf{y}}(\|\mathbf{x}-\mathbf{y}\|, t-\tau) g(\mathbf{y},\tau)\, \mathrm{d}\sigma_\mathbf{y}\, \mathrm{d}\tau, \quad \mathbf{x} \in \Omega, \tag{29}$$

where g is an unknown density on Σ. By letting $\mathbf{x}$ approach the boundary surface from the inside of Ω and using the usual jump conditions, we arrive at

$$\left(-\frac{1}{2} + \mathscr{K}\right) g = f. \tag{30}$$

Once g has been determined, the double layer potential (29) must be evaluated on Γ to obtain the quantity needed in the evaluation of the shape gradient in (8).

The approximate solution of the boundary integral equations (27) and (30) by traditional discretization schemes poses serious difficulties since the total number of unknowns is the product of the number of spatial unknowns N_s and temporal unknowns N_t which becomes extremely large. Therefore, we proposed in [17, 18] the application of the multipole-based space-time boundary element method which has been developed in [34, 35]. We then arrive at an algorithm which computes both, the state and its adjoint, in a complexity that scales essentially linearly with the total number of unknowns $N_s N_t$. We refer the reader to [17] for further details concerning the particular realization.

5.2 Solving the Poisson equation

In case of the Laplacian, the fundamental solution is $G(r) = 1/(4\pi r)$. Hence, the standard boundary integral operators (cf. (24)) become

$$\left.\begin{aligned}
(\mathscr{V}g)(\mathbf{x}) &= \int_\Sigma G(\|\mathbf{x}-\mathbf{y}\|)g(\mathbf{y})\,\mathrm{d}\sigma_{\mathbf{y}} \\
(\mathscr{K}g)(\mathbf{x}) &= \int_\Sigma \frac{\partial G}{\partial \mathbf{n}_{\mathbf{y}}}(\|\mathbf{x}-\mathbf{y}\|)g(\mathbf{y})\,\mathrm{d}\sigma_{\mathbf{y}} \\
(\mathscr{K}^\star g)(\mathbf{x}) &= \int_\Sigma \frac{\partial G}{\partial \mathbf{n}_{\mathbf{x}}}(\|\mathbf{x}-\mathbf{y}\|)g(\mathbf{y})\,\mathrm{d}\sigma_{\mathbf{y}} \\
(\mathscr{W}g)(\mathbf{x}) &= -\frac{\partial}{\partial \mathbf{n}_{\mathbf{x}}}\int_\Sigma \frac{\partial G}{\partial \mathbf{n}_{\mathbf{y}}}(\|\mathbf{x}-\mathbf{y}\|)g(\mathbf{y})\,\mathrm{d}\sigma_{\mathbf{y}}
\end{aligned}\right\} \quad \mathbf{x}\in\Sigma.$$

The Dirichlet and Neumann data at Σ are again coupled by the boundary integral equations (25), which, in view of the homogeneous boundary conditions, results in the boundary integral equations (27). The Newton potential involved there can be computed as follows:

Lemma 1. *For $\mathbf{x}\in\mathbb{R}^3\setminus\overline{D}$, the Newton potential admits the representation*

$$\mathscr{N}(\mathbf{x}) := \int_D G(\|\mathbf{x}-\mathbf{y}\|)\,\mathrm{d}\mathbf{y} = -\frac{1}{8\pi}\int_\Gamma \frac{\langle \mathbf{x}-\mathbf{y},\mathbf{n}_{\mathbf{y}}\rangle}{\|\mathbf{x}-\mathbf{y}\|}\,\mathrm{d}\sigma_{\mathbf{y}}.$$

Proof. We shall write the Laplace kernel as the divergence of a radially symmetric vector field. That is, we find a scalar function $F(\cdot)$ such that

$$\mathrm{div}_{\mathbf{y}}\Big[F(\|\mathbf{x}-\mathbf{y}\|)(\mathbf{x}-\mathbf{y})\Big] = G(\|\mathbf{x}-\mathbf{y}\|).$$

Simple differentiation shows that $F(\cdot)$ satisfies the differential equation in r

$$rF'(r)+3F(r) = -G(r), \quad r>0.$$

A particular solution of this ordinary differential equation is $F(r) = -1/(8\pi r)$. Thus, by construction, the Gauss theorem implies the assertion:

$$\int_D G(\|\mathbf{x}-\mathbf{y}\|)\,\mathrm{d}\mathbf{x} = \int_\Gamma F(\|\mathbf{x}-\mathbf{y}\|)\langle \mathbf{x}-\mathbf{y},\mathbf{n}_{\mathbf{y}}\rangle\,\mathrm{d}\sigma_{\mathbf{y}}.$$

□

We will employ the first boundary integral equation in (27) for the shape reconstruction scheme, since it is more accurate when applying a Galerkin method. Moreover, for the adjoint state, it is then more efficient to use the indirect method for the single layer potential, i.e.,

$$p(\mathbf{x}) = \int_\Sigma G(\|\mathbf{x}-\mathbf{y}\|)g(\mathbf{y})\,\mathrm{d}\sigma_{\mathbf{y}}, \quad \mathbf{x}\in\Omega. \tag{31}$$

Here, the density g is the solution of the boundary integral equation $\mathscr{V}g = f$ with the right hand $f(\mathbf{x}) := (\partial u/\partial\mathbf{n})(\mathbf{x}) - h(\mathbf{x})$.

As proposed in several earlier papers on shape optimization with elliptic state equation, see e.g. [5, 6, 7, 8], the present boundary integral equations can be solved

efficiently by the wavelet Galerkin method which has been developed in [1, 15]. Then, the computational complexity scales linearly in the number of boundary elements.

6 Numerical results

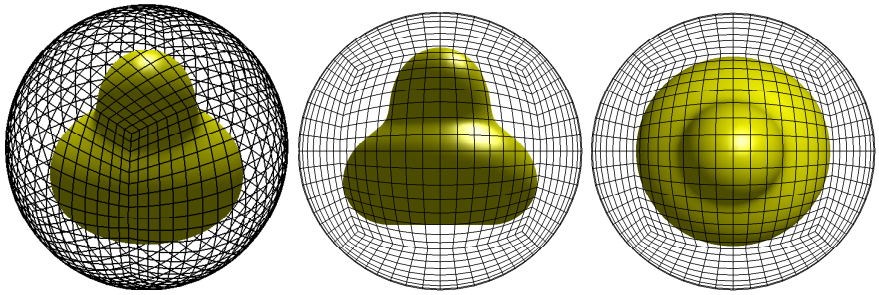

Fig. 3 The domain Ω with boundary Σ and the acorn-shaped source D with boundary Γ.

We shall illustrate our algorithms by some numerical experiments. To that end, we choose the unit ball as computational domain Ω. The given heat source D is acorn-shaped as shown in Figure 3. Since it is star-shaped, we employ the ansatz (20) with $N = 10$, that are 100 design parameters.

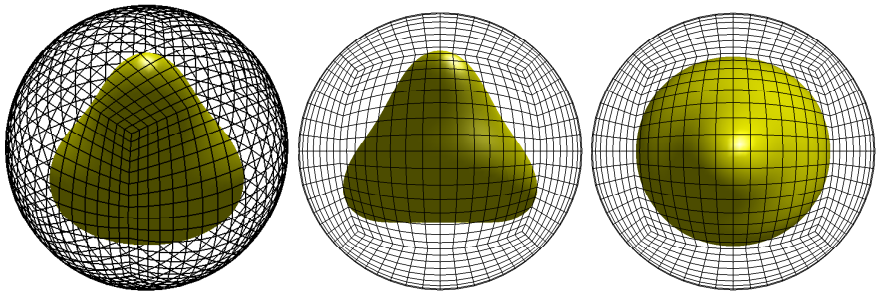

Fig. 4 The reconstruction of the heat source D in case of the heat equation and $T = 0.1$.

We apply first the reconstruction algorithm for the time interval $[0,T]$ with $T = 0.1$ and $T = 1.0$ and a noise level of 1%. It turns out that the reconstruction for the short time interval (see Figure 4) is quite similar but somewhat worse than for the long time interval (see Figure 5). This has nevertheless already been observed in [17].

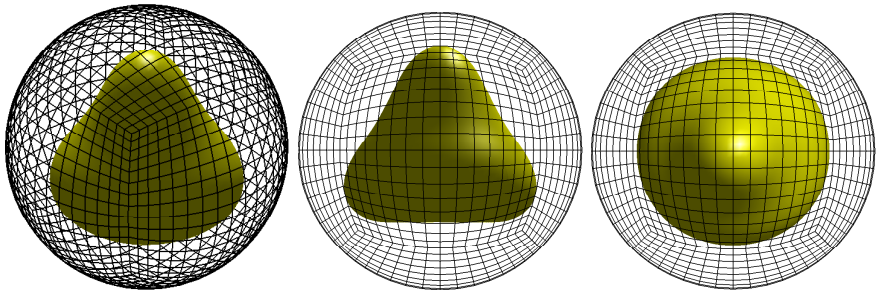

Fig. 5 The reconstruction of the heat source D in case of the heat equation and $T = 1.0$.

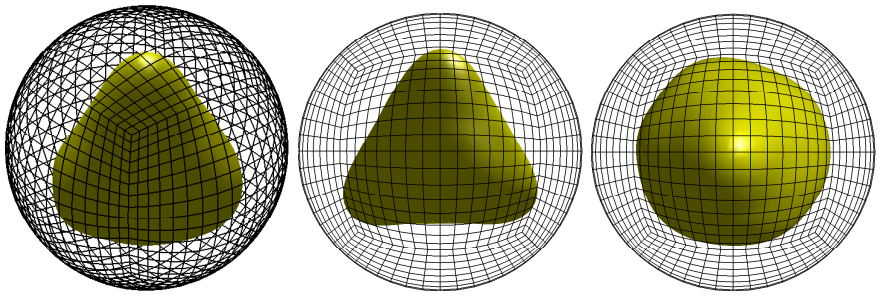

Fig. 6 The reconstruction of the heat source D in case of the stationary problem.

The reconstruction for the stationary situation is seen in Figure 6. Its quality is clearly inferior to the time-dependent problem. Moreover, we have observed that the reconstruction is much more robust with respect to noise if the time dependent heat flux is used in the tracking functional rather than the stationary heat flux.

References

1. W. Dahmen, H. Harbrecht and R. Schneider. Compression techniques for boundary integral equations. Optimal complexity estimates. *SIAM J. Numer. Anal.* **43** (2006) 2251–2271.
2. M. Delfour and J.-P. Zolesio. *Shapes and geometries*. SIAM, Philadelphia, 2001.
3. J.E. Dennis and R.B. Schnabel. *Numerical methods for nonlinear equations and unconstrained optimization techniques*. Prentice-Hall, Englewood Cliffs, 1983.
4. S. El Yacoubi and J. Sokolowski. Domain optimization problems for parabolic control systems. *Appl. Math. Comput. Sci.* **6** (1996) 277–289.
5. K. Eppler and H. Harbrecht. Numerical solution of elliptic shape optimization problems using wavelet-based BEM. *Optim. Methods Softw.* **18** (2003) 105–123.
6. K. Eppler and H. Harbrecht. A regularized Newton method in electrical impedance tomography using shape Hessian information. *Control Cybern.* **34** (2005) 203–225.
7. K. Eppler and H. Harbrecht. Efficient treatment of stationary free boundary problems. *Appl. Numer. Math.* **56** (2006) 1326–1339.

8. K. Eppler and H. Harbrecht. Wavelet based boundary element methods in exterior electromagnetic shaping. *Eng. Anal. Bound. Elem.* **32** (2008) 645–657.
9. K. Eppler, H. Harbrecht, and R. Schneider. On convergence in elliptic shape optimization. *SIAM J. Control Optim.* **45** (2007) 61–83.
10. A.V. Fiacco and G.P. McCormick. *Nonlinear programming. Sequential unconstrained minimization techniques*. Wiley, New York, 1968.
11. R. Fletcher. *Practical methods for optimization I&II*. Wiley, New York, 1980.
12. C. Grossmann and J. Terno. *Numerik der Optimierung*. B.G. Teubner, Stuttgart, 1993.
13. H. Harbrecht. Analytical and numerical methods in shape optimization. *Math. Methods Appl. Sci.* **31** (2008) 2095–2114.
14. H. Harbrecht. A Newton method for Bernoulli's free boundary problem in three dimensions. *Computing* **82** (2008) 11–30.
15. H. Harbrecht and R. Schneider. Wavelet Galerkin schemes for boundary integral equations. Implementation and quadrature. *SIAM J. Sci. Comput.* **27** (2006) 1347–1370.
16. H. Harbrecht and T. Hohage. Fast methods for three-dimensional inverse obstacle scattering. *J. Integral Equations Appl.* **19** (2007) 237–260.
17. H. Harbrecht and J. Tausch. An efficient numerical method for a shape identification problem arising from the heat equation. *Inverse Problems* **27** (2011) 065013.
18. H. Harbrecht and J. Tausch. On the numerical solution of a shape optimization problem for the heat equation. *SIAM J. Sci. Comput.* **35** (2013) A104–A121.
19. J. Haslinger and P. Neitaanmäki. *Finite element approximation for optimal shape, material and topology design*, 2nd edition. Wiley, Chichester, 1996.
20. A. Henrot and J. Sokolowski. A shape optimization problem for the heat equation. In *Optimal control (Gainesville, FL, 1997)*, pages 204–223. Volume 15 of *Applied Optimization*, Kluwer Acad. Publ., Dordrecht, 1998.
21. K.-H. Hoffmann and J. Sokolowski. Interface optimization problems for parabolic equations. Shape design and optimization. *Control Cybernet.* **23** (1994) 445–451.
22. F. Hettlich and W. Rundell. The determination of a discontinuity in a conductivity from a single boundary measurement. *Inverse Problems* **14** (1998) 67–82.
23. F. Hettlich and W. Rundell. Identification of a discontinuous source in the heat equation. *Inverse Problems* **17** (2001) 1465–1482.
24. V. Isakov. *Inverse Source Problems*. Volume 34 of *AMS Mathematical Surveys and Monographs*, American Mathematical Society, Providence RI, 1990.
25. K. Ito, K. Kunisch, and G. Peichl. Variational approach to shape derivatives for a class of Bernoulli problems. *J. Math. Anal. Appl.* **314** (2006) 126–149.
26. A.M. Khludnev and J. Sokołowski. *Modeling and control in solid mechanics*. Birkhäuser, Basel, 1997.
27. F. Murat and J. Simon. Étude de problèmes d'optimal design. In *Optimization Techniques, Modeling and Optimization in the Service of Man*, edited by J. Céa, pages 54–62. Volume 41 of *Lect. Notes Comput. Sci.*, Springer, Berlin, 1976.
28. O. Pironneau. *Optimal shape design for elliptic systems*. Springer, New York, 1983.
29. J.-R. Roche and J. Sokolowski. Numerical methods for shape identification problems. *Control Cybern.* **25** (1996) 867–894.
30. J. Simon. Differentiation with respect to the domain in boundary value problems. *Numer. Funct. Anal. Optimization* **2** (1980) 649–687.
31. J. Sokolowski. Shape sensitivity analysis of boundary optimal control problems for parabolic systems. *SIAM J. Control Optim.* **26** (1988) 763–787.
32. J. Sokolowski and J.-P. Zolesio. *Introduction to Shape Optimization*. Springer, Berlin, 1992.
33. T. Tiihonen. Shape optimization and trial methods for free-boundary problems. *RAIRO Model. Math. Anal. Numér.* **31** (1997) 805–825.
34. J. Tausch. A fast method for solving the heat equation by layer potentials. *J. Comp. Phys.* **224** (2007) 956–969.
35. J. Tausch. Nyström discretization of parabolic boundary integral equations. *Appl. Numer. Math.* **59** (2009) 2843–2856.

LATEST PREPRINTS

No.	Author: *Title*
2013-01	**H. Harbrecht, M. Peters** *Comparison of Fast Boundary Element Methods on Parametric Surfaces*
2013-02	**V. Bosser, A. Surroca** *Elliptic logarithms, diophantine approximation and the Birch and Swinnerton-Dyer conjecture*
2013-03	**A. Surroca Ortiz** *Unpublished Talk: On some conjectures on the Mordell-Weil and the Tate-Shafarevich groups of an abelian variety*
2013-04	**V. Bosser, A. Surroca** *Upper bound for the height of S-integral points on elliptic curves*
2013-05	**Jérémy Blanc, Jean-Philippe Furter, Pierre-Marie Poloni** *Extension of Automorphisms of Rational Smooth Affine Curves*
2013-06	**Rupert L. Frank, Enno Lenzmann, Luis Silvestre** *Uniqueness of Radial Solutions for the Fractional Laplacian*
2013-07	**Michael Griebel, Helmut Harbrecht** *On the convergence of the combination technique*
2013-08	**Gianluca Crippa, Carlotta Donadello, Laura V. Spinolo** *Initial-Boundary Value Problems for Continuity Equations with BV Coefficients*
2013-09	**Gianluca Crippa, Carlotta Donadello, Laura V. Spinolo** *A Note on the Initial-Boundary Value Problem for Continuity Equations with Rough Coefficients*
2013-10	**Gianluca Crippa** *Ordinary Differential Equations and Singular Integrals*
2013-11	**G. Crippa, M. C. Lopes Filho, E. Miot, H. J. Nussenzveig Lopes** *Flows of Vector Fields with Point Singularities and the Vortex-Wave System*
2013-12	**L. Graff, J. Fender, H. Harbrecht, M. Zimmermann** *Key Parameters in High-Dimensional Systems with Uncertainty*
2013-13	**Jérémy Blanc, Immanuel Stampfli** *Automorphisms of the Plane Preserving a Curve*

LATEST PREPRINTS

No. **Author:** *Title*

2013-14 **Jérémy Blanc, Jung Kyu Canci**
Moduli Spaces of Quadratic Rational Maps with a Marked Periodic Point of Small Order

2013-15 **Marcus J. Grote, Johannes Huber, Drosos Kourounis, Olaf Schenk**
Inexact Interior-Point Method for Pde-Constrained Nonlinear Optimization

2013-16 **Helmut Harbrecht, Florian Loos**
Optimization of Current Carrying Multicables

2013-17 **Daniel Alm, Helmut Harbrecht, Ulf Krämer**
The H^2-Wavelet Method

2013-18 **Helmut Harbrecht, Michael Peters, Markus Siebenmorgen**
*Multilevel Accelerated Quadrature for PDEs With Log-Normal Distributed Random Coefficient**

2013-19 **Jérémy Blanc, Serge Cantat**
Dynamical Degrees of Birational Transformations of Projective Surfaces

2013-20 **Jérémy Blanc, Frédéric Mangolte**
Cremona Groups of Real Surfaces

2013-21 **Jérémy Blanc, Igor Dolgachev**
Automorphisms of Cluster Algebras of Rank 2

2013-22 **Helmut Harbrecht, Giannoula Mitrou**
Improved Trial Methods for a Class of Generalized Bernoulli Problems

2013-23 **Helmut Harbrecht, Johannes Tausch**
On Shape Optimization with Parabolic State Equation